RSC Advances

PAPER

View Article Online
View Journal | View Issue

Cite this: *RSC Adv.*, 2021, **11**, 29178

Hydrothermal synthesis of nitrogen-doped carbon quantum dots from lignin for formaldehyde determination†

Ying Wang, Yushan Liu, Jin Zhou, Jinquan Yue, Mingcong Xu, Bang An, Chunhui Ma, Wei Li* and Shouxin Liu*

This work assessed the fabrication of nitrogen-doped CQDs (NCQDs) from alkali lignin (AL) obtained from spruce, representing a green, low-cost biomass generated by the pulp and biorefinery industries. The AL was found to retain its original lignin skeleton and could be used to produce NCQDs with excellent photoluminescence properties by one-pot hydrothermal treatment of AL and *m*-phenylenediamine. These NCQDs exhibited blue-green fluorescence (FL) with excitation/emission of 390/490 nm under optimal conditions. The NCQDs showed pH and excitation wavelength-dependent FL emission behaviors. On the basis of the exceptional selective response of these NCQDs to specific solvents, we developed a FL probe for the detection of formaldehyde (FA). The FL intensity of NCQDs was found to be directly proportional to the concentration of FA in the range of 0.05 to 2 mM (R^2 = 0.993), with a detection limit of 4.64 μM (based on $3\sigma/K$). A composite film comprising NCQDs with poly(vinyl alcohol) was found to act as a sensor with a good FL response to FA gas. When exposed to gaseous FA, this film exhibited increased FL intensity and transitioned from blue-green to blue. A mechanism is proposed in which the NCQDs react rapidly with FA to generate Schiff bases that result in enhanced FL emission and the observed blue shift in color.

Received 13th July 2021
Accepted 20th August 2021

DOI: 10.1039/d1ra05370a

rsc.li/rsc-advances

1. Introduction

Formaldehyde (FA) is a common indoor pollutant that can be emitted by building materials as well as by industrial manufacturing.[1,2] Elevated concentrations of airborne FA cause respiratory disease, central nervous system damage and even an increased risk of cancer.[3] Various methods have been reported for the detection of gaseous FA, such as electrochemical analysis,[4] spectroscopy,[5] chemiluminescence.[6] However, these techniques are typically expensive, complex and time consuming. Therefore, it would be beneficial to identify a low-cost, convenient and sensitive assay for the determination of FA.

Compared with other methods, fluorescence (FL) sensors are advantageous with regard to FA detection because they are less costly, highly sensitive and selective. Carbon quantum dots (CQDs) are widely used as sensors for analytical detectors because of their excellent optical properties, low toxicity and ease of functionalization,[7] and FL sensors based on CQDs for FA detection have been reported. Qu *et al.* successfully prepared N, P-co-doped CQDs using *N*-(phosphonomethyl)iminodiacetic acid and branched polyethyleneimine as precursors, and reported highly sensitive and selective intracellular FA sensing using this material.[8] Liu *et al.* successfully synthesized CQDs from dexamethasone and 1,2,4,5-tetraaminobenzene by microwave-assisted hydrothermal method, and successfully applied it to ratiometric fluorescence bioimaging of FA fluctuation in lysosome of living cells.[9] The majority of the CQDs used in FL sensors to date have been synthesized from low molecular weight organic molecules. Unfortunately, most organic molecules are not only expensive but also toxic: for example, polycyclic aromatic hydrocarbons (PAHs) are strong carcinogens, which pose a challenge to the natural environment and human health.[10] Facing this challenge, it is necessary find low-cost and environmentally friendly molecular precursors. In accordance with the principles of green sustainability, efforts have been made to develop low-cost and renewable biomass materials as precursors, such as cellulose,[11] citric acid,[12] sucrose,[13] milk,[14] and others. However, few biomass precursors can be prepared into high quality CQDs. Therefore, it is necessary to prepare high quality CQDs using low-cost, renewable and non-toxic biomass precursors.

Lignin, one of the most abundant natural sources on the earth, which has a high carbon content, a complex aromatic skeleton structure and a high oxygen-containing functional groups branches, all of which favor the formation CQDs based

Key Laboratory of Bio-based Material Science &Technology, Northeast Forestry University, Ministry of Education, Harbin 150040, P. R. China. E-mail: liwei19820927@126.com; liushouxin@126.com

† Electronic supplementary information (ESI) available. See DOI: 10.1039/d1ra05370a

on conjugated graphite-based nuclei with surface functionalization.[15,16] Therefore, lignin is considered a desirable raw material for the synthesis of CQDs. However, the value of lignin has not been widely exploited, which is a considered as a waste by-product in the pulp industry and cellulosic ethanol biorefineries.[17] In the past studies, lignin have been reported as carbon precursors to prepare of CQDs. For instance, Ding *et al.* prepared blue luminescent graphene quantum dots using alkali lignin as a precursor by sonication in nitric acid and hydrothermal treatment, and successfully used them for cell imaging.[18] Shi *et al.* obtained blue fluorescent CQDs by heating aminated lignin at 300 °C under a nitrogen atmosphere for 2 h, and applied these dots to the detection of Fe ions as well as cell imaging.[19] However, this material had several disadvantages, including weak FL intensity and a labor-intensive preparation process. Therefore, the synthesis of high-quality CQDs for FA detection using a simple and environmentally-friendly process with lignin as a precursor remains a challenge.

In the present work, nitrogen-doped CQDs (NCQDs) were obtained using a one-pot hydrothermal method, employing alkali lignin (AL) extracted from black pulp liquor as a precursor and *m*-phenylenediamine (MPDA) as a nitrogen source. These NCQDs exhibited exceptional selectivity and could be used as a FL probe for the detection of FA, giving a good calibration R^2 value of 0.993. This material was applied to the analysis of FA at concentrations between 0.05 and 2 mM and was determined to have a limit of detection (LOD) of 4.64 μM. A sensor made from a composite film comprising these NCQDs combined with poly(vinyl alcohol) (PVA) was fabricated and possessed an obvious response towards gaseous FA.

2. Experimental

2.1 Materials

Spruce wood was purchased from a local factory in Heilongjiang Province, China. NaOH and Na_2S were purchased from the Fuchen Chemical Reagent Co. (Tianjin, P. R. China). H_2SO_4 was purchased from the Comeo Chemical Reagent Co., Ltd. (Tianjin, P. R. China). FA, ethanol, methanol, acetone, dimethylsulfoxide (DMSO) and dimethylformamide (DMF) were obtained from the Guangfu Technology Development Co., Ltd. (Tianjin, P. R. China). The MPDA and PVA were bought from Aladdin Ltd. (Shanghai, P. R. China). All reagents were analytical grade and were used directly without further purification.

2.2 Preparation of alkali lignin

AL was extracted and purified from the black liquor generated by processing spruce pulp.[20–24] The spruce wood was first processed into strips approximately 5 × 0.5 × 0.5 cm in size, after which black liquor was extracted from the spruce wood using the same methods applied during the pulp making process. In a typical procedure, a 1000 g quantity of the spruce strips was combined with 145.3 g NaOH, 52.6 g Na_2S and 6 L water, after which the mixture was heated in a cooker at 170 °C for 2.5 h and the crude AL was obtained from the black liquor by acid precipitation. This was performed by first purifying and then filtering the liquor to remove fibers and other impurities, after which the pH of the black liquor was adjusted to 2.0 with 10 wt% H_2SO_4 in a 60 °C water bath to precipitate the lignin. This material was subsequently washed two or three times with deionized water (DI) and then dried at 40 °C under vacuum to obtain the crude AL. The crude AL was then extracted in a Soxhlet apparatus with a mixture of dioxane and DI (9 : 1 v/v) for 1.5 h, after which the extract was concentrated to a volume of 20–50 mL in a rotary evaporator under reduced pressure at 50 °C. This concentrated extract was added dropwise to ether to precipitate the AL, following which the ether was removed by washing with DI and the product was dried in a vacuum desiccator (with P_2O_5 as the desiccant) at 40 °C to obtain the pure AL.

2.3 Synthesis of NCQDs

NCQDs were prepared *via* the hydrothermal carbonization of the AL combined with MPDA. Typically, 0.1 g AL and 0.2 g MPDA were added into 15 mL DI and the mixture was transferred into a 50 mL Teflon autoclave and heated at 220 °C for 10 h. The NCQDs in powder form were obtained by bag dialysis in DI over a time span of 48 h (with a molecular weight cut off of 1000 Da) and then freeze-dried.

2.4 Preparation of NCQDs/PVA composite films

In a typical procedure, 3 g PVA was mixed with 60 mL DI and the mixture stirred continuously at 60 °C until the PVA was completely dissolved. Subsequently, 0.5 mg NCQDs was added to the PVA solution, followed by sonication for 10 min and stirring for another 30 min to obtain a homogeneous dispersion. Finally, 3 mL of this mixture was transferred to a plastic mold (3 cm in diameter) and dried under vacuum for 12 h to obtain an NCQDs/PVA composite film.

2.5 Detection of FA

To assess the analysis of FA *via* FL using these NCQDs, the effects of various solvents on the FL characteristics of this material were investigated. In each trial, a 40 μL portion of an aqueous dispersion of the NCQDs (Abs = 0.1) was added to 4 mL of water, FA, ethanol, methanol, acetone, DMSO or DMF and mixed for 1 min, after which the FL intensity of the NCQDs was measured. In each trial, the excitation was at 390 nm and the FL intensity was recorded at 490 nm. Trials were performed using various concentrations of FA in the range of 0 to 6 mM in conjunction with the NCQDs in aqueous dispersion. Finally, the detection of gaseous FA by the NCQDs/PVA composite membrane sensor was investigated. In these experiments, a 3 cm diameter portion of the NCQDs/PVA film and either 10 mL of a 37% FA solution were put into a vacuum desiccator. As comparison, trials were also performed with an NCQDs/PVA film and 10 mL of pure water in the vacuum desiccator. After 2.5 h, the FL intensity of the NCQDs/PVA sensor was assessed.

2.6 Characterization

The weight-average (M_w) and number-average (M_n) molecular weights of the AL were determined using gel permeation

chromatography (GPC, PL-GPC50, Agilent Technologies, USA). Two-dimensional heteronuclear single quantum coherence (2D-HSQC, III 400 MHz NMR, Bruker, Germany) spectra were acquired from AL samples of approximately 60 mg dissolved in 0.5 mL DMSO-d_6.[25] Ultraviolet-visible (UV-vis) absorption spectra of the NCQDs were also recorded (TU-1950, Purkinje, China). The FL emissions of the NCQDs were assessed using an FL spectrophotometer (F-7000, Agilent Technologies, USA) equipped with a 150 W xenon lamp as the excitation source. The structures of the NCQDs were examined by transmission electron microscopy (TEM) and high-resolution TEM (HRTEM) using an instrument (JEM 2100, JEOL Ltd., Japan) at an accelerating voltage of 200 kV. Fourier transform infrared (FT-IR) spectra of the NCQDs were obtained (iS10, Nicolet, USA), and X-ray photoelectron spectroscopy (XPS) data were obtained (Escalab 250 XI, TERMO, USA) using Al Kα radiation. X-ray diffraction (XRD) patterns were obtained with an instrument (D8, Bruker AXS, Germany) with a Cu Kα radiation source.

3. Results and discussion

3.1. Characterization of AL

Lignin is the second most abundant natural polymer in the world but is difficult to effectively use, and thus it is often a waste by-product of industries such as pulp manufacturing. Therefore, the present work mimicked the pulp making process to first obtain black liquor and then extract and purify AL. First of all, we used GPC to ascertain the M_w, M_n and polydispersity coefficient (M_w/M_n) of the AL (Table S1†). The resulting data are consistent with previous reports,[26] and indicate that the AL had a high molecular weight and a wide molecular weight distribution, which represents a challenge with regard to its use as a precursor for CQDs synthesis. Then, the AL structure was studied by FT-IR and 2D-HSQC spectroscopy.[26–28] The FT-IR (Fig. S1 and Table S2†) and 2D-HSQC (Fig. S2 and Table S3†) data demonstrated that the AL was relatively intact after processing and retained a complex aromatic structure having a high O-containing functional groups. This structure would be expected to promote the formation and surface functionalization of conjugated graphite nuclei in the NCQDs. Meanwhile, this structure allowed elemental doping to modify the physicochemical properties of the product.

3.2. Structural characteristics of the NCQDs

Phenylenediamine is often used as a source of nitrogen in the synthesis of CQDs because it can easily form conjugated N-containing groups.[29,30] Therefore, we prepared NCQDs by hydrothermal treatment of carbon source-AL and nitrogen source-MPDA (Scheme 1), and subsequently assessed the structure of this material by TEM and XRD. The TEM image in Fig. 1a clearly shows that the NCQDs were spherical and uniformly dispersed, with a size distribution of 1.3–3.2 nm. The HRTEM image in the inset to Fig. 1a demonstrates that the NCQDs generated well-resolved lattice stripes with a lattice spacing of approximately 0.21 nm, which was attributed to the (100) crystal planes of graphitic carbon.[31] Two diffraction peaks were present in the XRD pattern of the NCQDs (Fig. 1b) at 20.66° (d_{002} = 0.34 nm) and 42.56° (d_{100} = 0.21 nm). These results suggested that the NCQDs were composed of amorphous carbon phases and graphitic sp^2 carbon clusters, and confirmed the presence of abundant functional groups on the surfaces as well as carbon atoms in the graphite nuclei.

The chemical composition of the NCQDs was analyzed by FT-IR spectroscopy and XPS. The FT-IR spectrum in Fig. 1c shows three peaks at 1600, 1510 and 1425 cm^{-1} associated with aromatic rings, indicating that the NCQDs were composed of aromatic skeletons. The absorption band at 1600 cm^{-1} was significantly enhanced compared with that in the AL spectrum (Fig. S1†), suggesting an increase in the amount of conjugated graphitic carbon in the NCQDs during the hydrothermal process, which is consistent with the HRTEM and XRD results. It is apparent that new peaks appeared at 3210, 1688, 1496 and 1378 cm^{-1} compared to lignin, which were attributed to N–H stretching vibrations, C=N vibrational absorption, NH_2 stretching vibrations and C–N bending vibrations, respectively. The results of the FT-IR analysis showed that the AL successfully synthesized NCQDs and that N was doped into the carbon backbone. It was also apparent that abundant functional groups appeared on the surfaces of the product.

The elemental composition of the NCQDs was further analyzed by XPS and the resulting spectrum contained three peaks at 287.0 eV (C 1s, 74.18%), 402.0 eV (N 1s, 6.17%) and 535.0 eV (O 1s, 19.65%) (Fig. S3†). The high-resolution C 1s spectrum is presented in Fig. 1d and can be deconvoluted into peaks related to C=C/C–C (284.2 eV), C–N (285.0 eV), C–O (286.1 eV) and C=O (288.4 eV). Fig. 1e shows the high-resolution O 1s spectrum, which can be deconvoluted into two peaks corresponding to C=O/–COOH (531.9 eV) and C–O (532.9 eV). In Fig. 1f, the N 1s peak can be divided into three peaks that are attributed to pyridinic N (398.2 eV), pyrrolic N (399.0 eV) and graphitic N (399.9 eV). These XPS data therefore provided further evidence that nitrogen was successfully doped

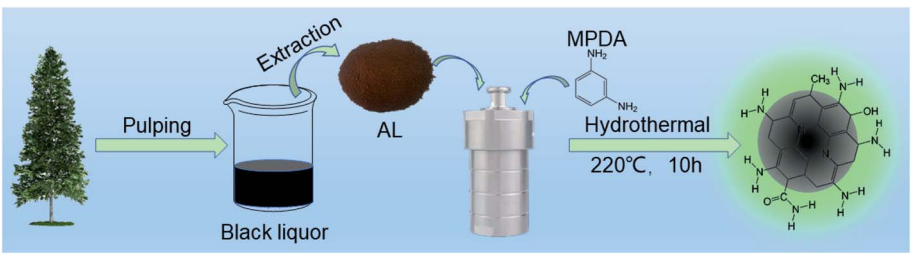

Scheme 1 Preparation process of NCQDs from alkaline lignin.

into the NCQDs structure along with the formation of many functional groups.

3.3. Optical properties of the NCQDs

The optical properties of NCQDs will have an important effect on their potential applications, and so the optical characteristics of the NCQDs were investigated. The inset of Fig. 2a provides an image of an NCQDs dispersion exhibiting blue-green FL emission at 365 nm. Seen from Fig. 2a, the UV-vis spectrum contained a typical absorption peak at 280 nm, which was attributed to the π–π* absorption band associated with the aromatic sp^2 structural region in the NCQDs. In this figure, the FL emission spectrum (labeled Em) and the corresponding FL excitation spectrum (labeled Ex) obtained from the NCQDs are presented, and show maxima at 390 and 490 nm, respectively. The emission wavelength and intensity of CQDs varies with the excitation wavelength, reflecting the effect of particles having different sizes in the fluorescent material and the distribution of different emission points on each nanoparticle.[32] As shown in Fig. 2b, the FL emission behavior of the NCQDs was assessed with excitation from 280 to 450 nm. When the excitation wavelength was in the range of 280–300 nm, NCQDs exhibited dual-emission behavior and the two peaks are located at 354 nm and 384 nm, respectively. These two peaks changed in intensity as the excitation wavelength changes, but the peak position remained the same. This excitation-independent FL emission behavior may be attributed to the π–π* transitions. However, when the excitation wavelength was more than 350 nm, the emission peak was gradually red-shifted with increases in the excitation wavelength. NCQDs showed the maximum excitation and emission wavelengths at 390 nm and 490 nm. Therefore, 390 nm was used as the optimal excitation wavelength in the subsequent experiments. This excitation-dependent FL emission may be attributed to the abundant functional groups on the surfaces of the NCQDs.[12]

The FL behavior of the NCQDs was also examined at various pH values and in different solvents. The pH of an aqueous dispersion of the NCQDs was adjusted using either 3 M HCl or 1 M NaOH and, as shown in Fig. S4,† the FL intensity slowly decreased under acidic conditions but decreased more sharply under alkaline conditions. This may have been caused by the increases in negative charges on the NCQDs surfaces at higher pH values, which would have inhibited the migration of electrons and thus resulted in a greater decrease in the FL intensity. Furthermore, seen from Fig. 2c, the FL emission peak was blue-shifted under alkaline conditions, indicating that pH also affected the FL emission centers in the NCQDs. This effect could possibly have been the result of the protonation/deprotonation of the pyridinic N-atoms such that the electrostatic interactions between the NCQDs shifted the Fermi energy levels and affected the FL emission centers of the NCQDs.[33–36] Previous studies have shown that N-doped CQDs may show different FL emission properties based on their interactions with the surrounding medium.[37] Therefore, the luminescence behavior of the NCQDs was assessed in six different solvents (Fig. 2d). The data showed that the FL intensity was significantly greater in the presence of FA compared with the other solvents, possibly because the numerous oxygen-containing functional groups on the NCQDs surfaces promoted the adsorption of electrons from the solvent molecules. It is also possible that the NCQDs underwent coordination interactions with the solvent molecules that varied the FL emission intensity and emission centers.[38,39] These

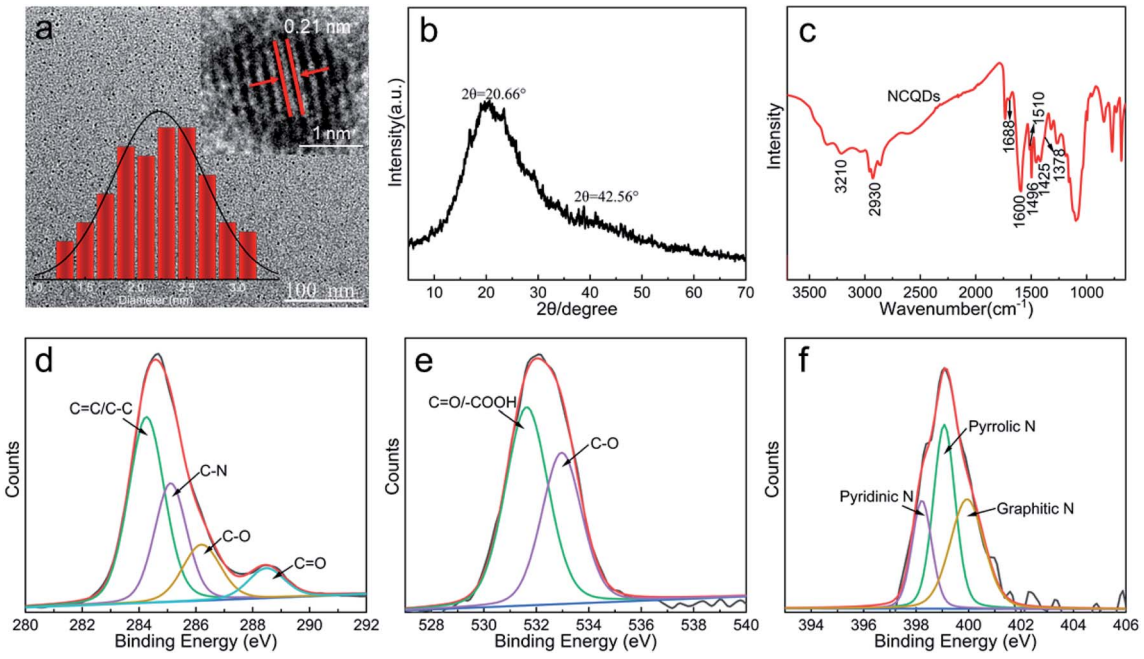

Fig. 1 (a) TEM (HRTEM) images and size distribution histograms of the NCQDs (inset); (b) XRD pattern and (c) FT-IR spectra of the NCQDs. (d) High-resolution C 1s peaks; (e) high-resolution O 1s peaks; (f) high-resolution N 1s peaks.

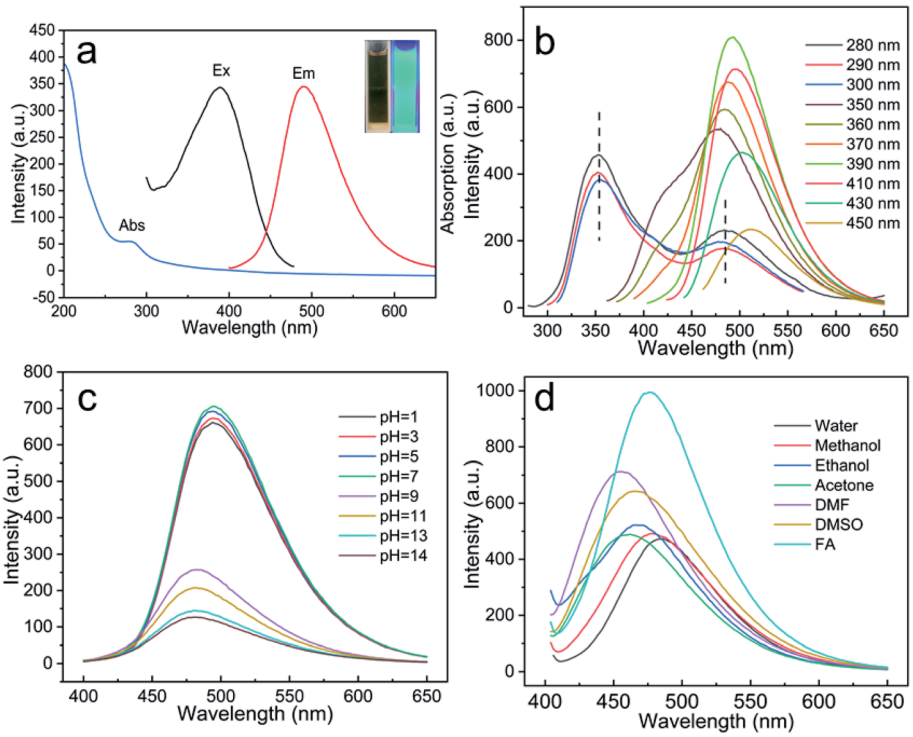

Fig. 2 (a) UV-vis absorption, Em (emission wavelength = 490 nm) and Ex spectra (excitation wavelength = 390 nm), inset (a) shows a digital photograph of the NCQDs under 365 nm UV light. (b) FL emission spectra of the NCQDs at different excitation wavelengths. (c) FL emission spectra of the NCQDs at different solution pH values (excited at 390 nm). (d) FL emission spectrum of NCQDs aqueous solution mixed with different solvents (excited at 390 nm).

variations in the FL emission with pH and solvent demonstrate the feasibility of applications related to pH sensors and FA detection.

3.4. FA detection

On the basis of the selective sensing of the NCQDs for FA (Fig. S5†), a sensor design was developed. As shown in Fig. 3a,

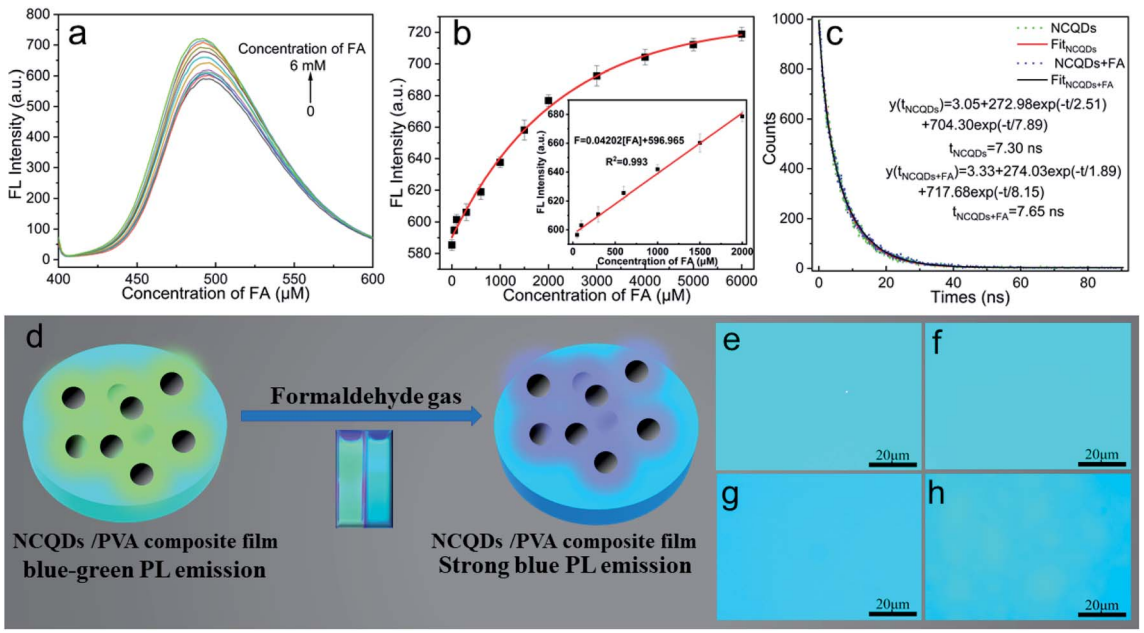

Fig. 3 (a) FL emission spectra of NCQDs solutions at different concentrations of FA (from bottom to top 0, 0.05, 0.1, 0.3, 0.6, 1, 1.5, 2, 3, 4, 5, and 6 mM under excitation at 390 nm). (b) FL intensity as a function of FA concentration. (c) Fluorescence lifetime decay of NCQDs before and after reaction with FA. (d) Schematic of FA gas sensing by NCQDs/PVA composite film. FL microscopy images of NCQDs/PVA composite film under excitation by UV light treated with (e) normal air, (f) water gas, and (g) FA gas. (h) FA gas to air environment.

the FL emission intensity generated by the NCQDs was enhanced with increasing concentrations of FA, while the maximum emission peak was blue-shifted. Moreover, the emission intensity exhibited a good linear correlation with the FA concentration (Fig. 3b). The linear regression equation for this relationship was intensity = 0.04202[FA] + 596.965 (over the range of 0.05 mM to 2 mM), and the linear regression coefficient was $R^2 = 0.993$. The LOD for FA was estimated to be 4.64 μM (based on $3\sigma/K$). The average fluorescence lifetime of NCQDs was 7.30 ns, and the average fluorescence lifetime after treatment with FA was determined to be 7.65 ns, which is larger than that of free NCQDs (Fig. 3c). In the present work, the NCQDs were combined with PVA to prepare an NCQDs/PVA composite film as a sensor for gaseous FA (Fig. 3d), and Fig. S6† shows images of composite specimens that weak blue-green and blue FL in air and FA gas, respectively, under 365 nm excitation. The effectiveness of the NCQDs/PVA composite film was examined by placing the sample in a vacuum desiccator and exposing the material to water vapor and FA gas. Fig. 3e and f shows that there were no significant changes in the FL emission intensity of the NCQDs/PVA composite film when exposed to ambient air and gaseous water. However, the FL emission intensity of the film was significantly enhanced upon exposure to gaseous FA and its color changed from blue-green to blue (Fig. 3g). As well, three sets of experiments were repeated and the same results were obtained (Fig. S7†). In addition, when the NCQDs/PVA composite film was removed from the FA gas environment and placed in the air environment for 10 min, the color of the composite film was unevenly colored (Fig. 3h). This may be attributed to the unstable binding product of FA and NCQDs in the composite film, which in turn decomposes into FA and volatilizes into the air. These results demonstrate that this NCQDs/PVA sensor concept could be used for visual FA gas sensing.

Compared with previously reported optical FA sensors, this device has several advantages, as shown in Table 1. First, the NCQDs are prepared from lignin, a low-cost green raw material, and the preparation method is relatively simple. Second, this sensor has a wider linear range and relatively low LOD. Third, it can react quickly with FA, has a lower cost of detection and simpler operation. Finally, the NCQDs can be readily compounded with PVA and the resulting composite film provides a prompt color-based response.

3.5. Possible mechanism

A possible mechanism for the enhanced FL and blue-shift of the NCQDs FL emission upon interaction with FA was examined, based on FTIR data and zeta potential characterizations. In these trials, a 15 mg quantity of the NCQDs was dispersed in 20 mL deionized water, after which 2 mL of an FA solution (37%) was added followed by 1 min of stirring. A yellow powder referred to herein as NCQDs-FA was subsequently isolated by vacuum drying of the dispersion, which was then characterized by FT-IR. As shown in Fig. 4a, compared with the original NCQDs, the C=N stretching peak generated by the NCQDs-FA at 1662 cm^{-1} was significantly enhanced. This is due to the reaction of NCQDs with FA to generate Schiff bases. To further demonstrate the generation of Schiff base, we measured the zeta potential of the NCQDs solution and the solution after the addition of FA (called NCQDs-FA solution). Since the weaker basicity of the C=N group as compared with the *o*-diamino-amine group, the zeta potential changes significantly with the generation of Schiff base. As shown in Fig. 4b, the zeta potential of NCQDs-FA solution changed significantly from −27.4 mV to −38.4 mV. FT-IR data and zeta potential characterizations are consistent with previous reports that the amine groups on NCQDs react rapidly with FA to form Schiff bases.[8,49] In addition, the NCQDs-FA powder was characterized by XPS. The N 1s spectra were analyzed, and the pyridinic N content increased significantly, while the graphite N content remained almost unchanged compared to NCQDs (Fig. S8 and Table S4†). Therefore, excluding possible interactions with N-atoms present in the honeycomb matrix of NCQDs. In a prior study,[50] CQDs in certain polar solvents (such as water, methanol and ethanol) formed stable intermolecular hydrogen bonds between $-NH_2$ groups on the surfaces of NCQDs and –OH groups in the solvents, resulting in the stabilization of excited states and produced significant FL quenching and red shifts. Therefore, we propose a possible mechanism (Fig. 4c) in which the NCQDs react rapidly with FA to produce Schiff bases such that the strong hydrogen bonding between the NCQDs and

Table 1 Comparative analysis of published various optical sensors for the determination of FA

Material	Reaction time	Medium used	Linear range	LOD	Ref.
AgNCs	150 min	Water	1–9 μM	0.14 μM	40
AgNCs@Tollens	1 min	Water	30–50 μM	27.99 μM	41
Eu^{3+}@Bio-MOF-1	—	Solid state	0–14 ppm	5.50 ppm	42
Compound 1	8 min	Phosphate-buffered solution (PBS)	—	0.78 μM	43
BPEI-CQDs	—	PBS buffer	0–40 μM	0.47 μM	8
FAP-1	120 min	PBS buffer	—	5 μM	44
Red CQDs	<1 min	PBS buffer	0–20 mM	9.9 μM	45
RFAP	120 min	PBS buffer	—	0.3 μM	46
DP5J-Bi_3	—	DMF	15–32 μM	3.27 nM	47
Zr-UiO-66-NH_2	2 min	Water	10–100 ppm	4.0 ppm	48
NCQDs	1 min	Water	0.05–2 mM	4.64 μM	This work

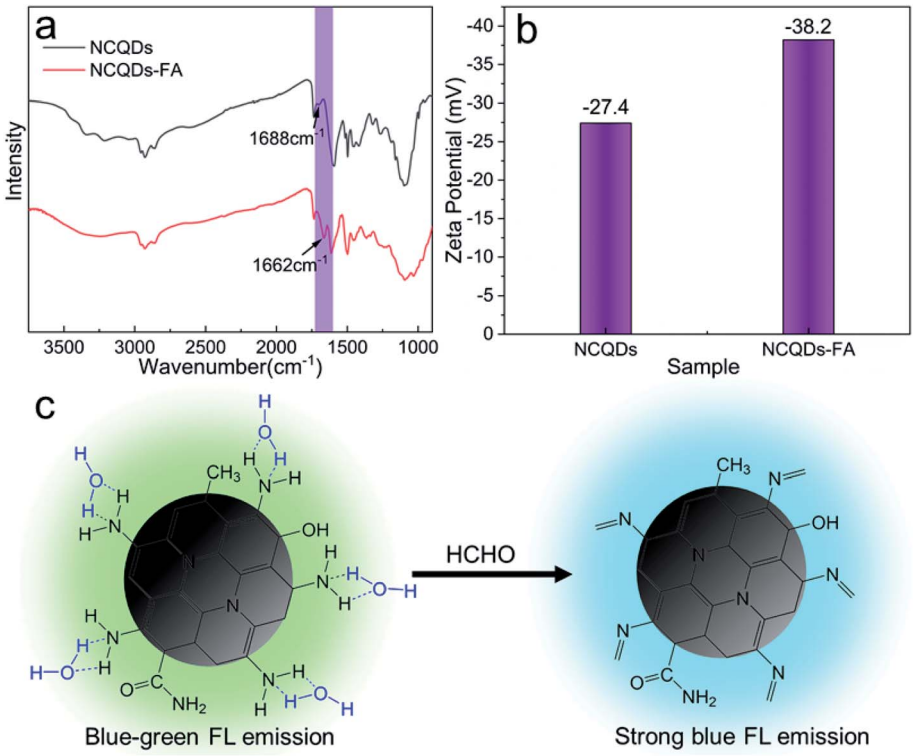

Fig. 4 (a) FT-IR contrast spectra of NCQDs and NCQDs-FA. (b) Zeta potential of NCQDs and NCQDs-FA. (c) Possible reaction mechanism of NCQDs towards FA.

water are disrupted, which leads to enhanced FL and a blue shift in the color of the NCQDs.

4. Conclusions

AL was successfully extracted from spruce as an inexpensive, green raw material. NCQDs were then fabricated by a simple one-pot hydrothermal method using AL as the carbon source and MPDA as the dopant. These NCQDs were almost monodisperse in water (with a size distribution in the range of 1.3–3.2 nm) and they exhibited significant FL that was affected by both the excitation wavelength and solution pH. The NCQDs were able to react rapidly with FA to form Schiff bases, which disrupted the hydrogen bonding interactions between the NCQDs and water, resulting in enhanced PL emission and a blue shift of their emission centers. Therefore, this material could be used as an effective FL probe for FA detection in the range of 0.05–2 mM, with a LOD of 4.64 μM. An NCQDs/PVA composite film sensor was designed that underwent a color change upon exposure to FA vapor. Currently, lignin is often regarded as a low value waste product because of its ineffective utilization. However, the current study indicates the conversion of lignin into high quality NCQDs with applications to FA analysis in keeping with the principles of sustainable development.

Author contributions

The authors Ying Wang, Yushan Liu, Jin Zhou, Mingcong Xu and Bang An involved in data collection, manuscript preparation and writing. The authors Jinquan Yue, Chunhui Ma, Wei Li, Shouxin Liu, helped in writing, reviewing, and editing the manuscript.

Conflicts of interest

The authors declare that they have no known competing financial interests or personal relationships that could have appeared to influence the work reported in this paper.

Acknowledgements

The present work was financially supported by the National Natural Science Foundation of China (32071719, 31890773) and the Natural Science Foundation of Heilongjiang Province (YQ2020C016). We thank Michael D. Judge, from Liwen Bianji, Edanz Editing China (http://www.liwenbianji.cn/ac), for editing the English text of a draft of this manuscript.

Notes and references

1 T. Salthammer, S. Mentese and R. Marutzky, *Chem. Rev.*, 2010, **110**, 2536–2572.
2 T. Salthammer, *Angew. Chem.*, 2013, **52**, 3320–3327.
3 H. A. Heck and M. Casanova, *Regul. Toxicol. Pharmacol.*, 2004, **40**, 92–106.
4 S. Zhang, L. Zhao, B. Huang and X. Li, *Sens. Actuators, B*, 2020, **319**, 128264.

5 P. Gorrotxategi-carbajo, E. Fasci, I. Ventrillard, M. Carras, G. Maisons and D. Romanini, *Appl. Phys. B: Lasers Opt.*, 2013, **110**, 309–314.
6 Y. Song, C. Gao, L. Qiao and S. Fan, *Chin. J. Lumin.*, 2009, **30**, 467–472.
7 R. Gui, H. Jin, Y. Wang and J. Sun, *Sens. Actuators, B*, 2017, **245**, 386–394.
8 J. Qu, X. Zhang, Y. Liu, Y. Xie and S. Jing, *Microchim. Acta*, 2020, **187**, 355.
9 H. Liu, Y. Sun, Z. Liu and J. Yang, *Nanoscale*, 2019, **11**, 8458–8463.
10 K. J. Mintz, Y. Q. Zhou and R. M. Leblanc, *Nanoscale*, 2019, **11**, 4634–4652.
11 P. Wu, W. Li, Q. Wu, Y. Liu and S. Liu, *RSC Adv.*, 2017, **7**, 44144–44153.
12 Y. Liu, S. Luo, P. Wu, C. Ma and S. Liu, *Anal. Chim. Acta*, 2019, **1090**, 133–142.
13 V. Gude, A. Das, T. Chatterjee and P. K. Mandal, *Phys. Chem. Chem. Phys.*, 2016, **18**, 28274–28280.
14 C. Zhu, J. Zhai and S. Dong, *Chem. Commun.*, 2012, **48**, 9367–9369.
15 B. Zhang, Y. Liu, M. Ren, W. Li, X. Zhang, R. Vajtai, P. M. Ajayan, J. M. Tour and L. Wang, *ChemSusChem*, 2019, **12**, 4202–4210.
16 M. Y. Si, Z. Jin, Y. Y. He and Z. Q. Yang, *Green Chem.*, 2018, **20**, 3414–3419.
17 D. Kai, M. J. Tan, P. L. Chee, Y. K. Chua, Y. L. Yap and X. J. Loh, *ChemInform*, 2016, **47**, 4202–4210.
18 Z. Y. Ding, F. F. Li, J. L. Wen and X. L. Wang, *Green Chem.*, 2018, **20**, 1383–1390.
19 Y. Shi, X. Liu, M. Wang, J. Huang, X. Jiang, J. Pang, F. Xu and X. Zhang, *Int. J. Biol. Macromol.*, 2019, **128**, 537–545.
20 A. Björkman, *Nature*, 1954, **174**, 1057–1058.
21 F. Xu, J. X. Sun, C. F. Liu and R. C. Sun, *Carbohydr. Res.*, 2006, **341**, 253–261.
22 A. Ziebell, K. Gracom, R. Katahira, F. Chen, Y. Pu, A. Ragauskas, R. A. Dixon and M. Davis, *J. Biol. Chem.*, 2010, **285**, 38961–38968.
23 A. Nadif, D. Hunkeler and P. Kauper, *Bioresour. Technol.*, 2002, **84**, 49–55.
24 M. L. Fidalgo, M. C. Terron, A. T. Martinez, A. E. Gonzalez and G. C. Galletti, *J. Agric. Food Chem.*, 1993, **41**, 1621–1626.
25 A. Rico, J. Rencoret, J. C. del Río, A. T. Martinez and A. Gutierrez, *Biotechnol. Biofuels*, 2014, **7**, 1–14.
26 Y. Zhang, J. Q. Wu, H. Li, T. Q. Yuan, Y. Y. Wang and R. C. Sun, *ACS Sustainable Chem. Eng.*, 2017, **5**, 7269–7277.
27 O. Faix, *Holzforschung*, 1991, **45**, 21–28.
28 F. Xu, R. C. Sun, M. Z. Zhai, J. X. Sun, J. X. Jiang and G. J. Zhao, *J. Appl. Polym. Sci.*, 2008, **108**, 1158–1168.
29 S. Sun, L. Zhang, K. Jiang, A. G. Wu and H. W. Lin, *Chem. Mater.*, 2016, **28**, 8659–8668.
30 H. Ding, S. B. Yu, J. S. Wei and H. M. Xiong, *ACS Nano*, 2016, **10**, 484–491.
31 Y. Liu, P. Wu, X. Wu, C. Ma, S. Luo, M. Xu, W. Li and S. Liu, *Talanta*, 2020, **210**, 120649.
32 B. P. Jiang, B. Zhou, X. C. Shen, Y. X. Yu, S. C. Ji, C. C. Wen and H. Liang, *Chem.–Eur. J.*, 2015, **21**, 18993–18999.
33 B. Vercelli, R. Donnini, F. Ghezzi, A. Sansonetti, U. Giovanella and B. L. Ferla, *Electrochim. Acta*, 2021, **387**, 138557.
34 M. Moniruzzaman and J. Kim, *Sens. Actuators, B*, 2019, **295**, 12–21.
35 A. Pyne, S. Layek, A. Patra and N. Sarkar, *J. Mater. Chem. C*, 2019, **7**, 6414–6425.
36 Z. Wu, M. Gao, T. Wang, X. Wan, L. Zheng and C. Huang, *Nanoscale*, 2014, **6**, 3868–3874.
37 P. Kumar and H. B. Bohidar, *J. Lumin.*, 2013, **141**, 155–161.
38 X. Shan, L. Chai, J. Ma, Z. Qian, J. Chen and H. Feng, *Analyst*, 2014, **139**, 2322–2325.
39 R. Zhang, Y. Liu, L. Yu, Z. Li and S. Sun, *Nanotechnology*, 2013, **24**, 225601.
40 K. Chaiendoo, S. Boonchiangma, V. Promarak and W. Ngeontae, *Colloid Polym. Sci.*, 2018, **296**, 1995–2004.
41 S. Nandi, E. Sharma, V. Trivedi and S. Biswas, *Inorg. Chem.*, 2018, 15149–15157.
42 Y. Zhang and B. Yan, *J. Mater. Chem. C*, 2019, **7**, 5652–5657.
43 H. Song, S. Rajendiran, N. Kim, S. K. Jeong, E. Koo, G. Park, T. D. Thangadurai and S. Yoon, *Tetrahedron Lett.*, 2012, **53**, 4913–4916.
44 T. F. Brewer and C. J. Chang, *J. Am. Chem. Soc.*, 2015, **137**, 10886–10889.
45 H. Wang, J. Wei, C. Zhang, Y. Zhang and J. Chen, *Chin. Chem. Lett.*, 2020, **31**, 759–763.
46 T. F. Brewer, G. Burgos-Barragan, N. Wit, K. J. Patel and C. J. Chang, *Chem. Sci.*, 2017, **8**, 4073–7081.
47 Q. Lin, Y. Q. Fan, G. F. Gong, P. P. Mao, J. Wang, X. W. Guan, J. Liu, Y. M. Zhang, H. Yao and T. B. Wei, *Chem. Eng.*, 2018, **6**, 8775–8781.
48 K. Vellingiri, A. Deep, K. H. Kim, D. W. Boukhvalov, P. Kumar and Q. Yao, *Sens. Actuators, B*, 2017, **241**, 938–948.
49 L. Wei, W. Tan, G. Wang, Q. Li and Z. Guo, *Carbohydr. Polym.*, 2019, **226**, 115256.
50 K. Jiang, S. Sun, L. Zhang, Y. Lu, A. Wu, C. Cai and H. Lin, *Angew. Chem., Int. Ed.*, 2015, **54**, 5360–5363.